ORIGINAL ARTICLE

Journal of Cachexia, Sarcopenia and Muscle 2022; **13**: 544–560
Published online 19 December 2021 in Wiley Online Library (wileyonlinelibrary.com) **DOI:** 10.1002/jcsm.12879

Cholesterol absorption blocker ezetimibe prevents muscle wasting in severe dysferlin-deficient and *mdx* mice

Zoe White[1,2], Marine Theret[3], Nadia Milad[1,2], Lin Wei Tung[3], William Wei-Han Chen[1,2], Martin G. Sirois[4], Fabio Rossi[3]* & Pascal Bernatchez[1,2]*

[1]*Department of Anesthesiology, Pharmacology & Therapeutics, University of British Columbia (UBC), Vancouver, BC, Canada;* [2]*UBC Centre for Heart Lung Innovation, St. Paul's Hospital, Vancouver, BC, Canada;* [3]*School of Biomedical Engineering, Department of Medical Genetics, University of British Columbia (UBC), Vancouver, BC, Canada;* [4]*Montreal Heart Institute, Department of Pharmacology and Physiology, Université de Montréal, Montreal, QC, Canada*

Abstract

Background Muscular dystrophy (MD) causes muscle wasting and is often lethal in patients due to a lack of proven therapies. In contrast, mouse models of MD are notoriously mild. We have previously shown severe human-like muscle pathology in *mdx* [Duchenne MD (DMD)] and dysferlin-deficient limb-girdle MD type 2B (LGMD2B) mice by inactivating the gene encoding for apolipoprotein E (ApoE), a lipid transporter synthesized by the liver, brain and adipocytes to regulate lipid and fat metabolism. Having recently established that human DMD is a novel type of primary genetic dyslipidaemia with elevated cholesterol, we sought to determine whether cholesterol could exacerbate the muscle wasting process observed in severe rodent MD.

Methods Severe *mdx* and dysferlin knock-out mice lacking ApoE were treated with ezetimibe (15 mg/kg/day), a clinically approved drug exhibiting few pleiotropic effects. In separate studies, dietary cholesterol was raised (from 0.2% to 2% cholesterol) in combination with experimental micro-injury and direct cholesterol injection assays. Muscles were assessed histologically for changes in collagen and adipocyte infiltration and both transcriptomic and cellular changes by RNA-seq and fluorescence-activated cell sorting analysis.

Results Treatment of severe DMD and LGMD2B mice with ezetimibe completely prevented clinical signs of ambulatory dysfunction (0% incidence vs. 33% for vehicle treatment; $P < 0.05$). Histological analyses revealed that ezetimibe-reduced fibro-fatty infiltration up to 84% and 63% in severely affected triceps ($P \leq 0.0001$) and gastrocnemius ($P \leq 0.003$) muscles, resulting in a respective 1.9-fold and 2.2-fold retention of healthy myofibre area ($P \leq 0.0001$). Additionally, raising dietary cholesterol and thus concentrations of plasma low-density lipoprotein-associated cholesterol (by 250%; $P < 0.0001$) reduced overall survivability (by 100%; $P < 0.001$) and worsened muscle damage in the LGMD2B triceps by 767% ($P < 0.03$). Micro-pin-induced mechanical injury in LGMD2B mice fed a high cholesterol diet exacerbated muscle damage by 425% ($P < 0.03$) and increased macrophage recruitment (by 98%; $P = 0.03$) compared with those injured on a chow diet. Parallel RNA-seq analyses revealed that injury in cholesterol-fed mice also modulated the expression of 3671 transcripts (1953 up-regulated), with fibrogenic, inflammatory and programmed cell death-associated pathways among the most enriched. Mice lacking dysferlin also displayed heightened muscle necrosis (by 123%; $P < 0.0001$) following a direct intramuscular injection of cholesterol compared with control mice.

Conclusions Cholesterol exacerbates rodent MD. Specific inhibition of cholesterol absorption with ezetimibe may safely attenuate human MD severity and delay death.

Keywords Dysferlin; Dystrophin; Cholesterol; Triglycerides; Plasma lipids

Received: 4 May 2021; Revised: 26 October 2021; Accepted: 29 October 2021
**Correspondence to: Pascal Bernatchez, Department of Anesthesiology, Pharmacology & Therapeutics, University of British Columbia, 217-2176 Health Sciences Mall, Vancouver, BC V6T 1Z3, Canada. Phone: 604-692-2344 x 66060, Fax: 604-806-9274, Email: pascal.bernatchez@ubc.ca; Fabio Rossi, Biomedical Research Centre, University of British Columbia (UBC), 2222 Health Sciences Mall, Vancouver, BC V6T 1Z3, Canada. Phone: 604-822-7138, Fax: 604-822-7815, Email: fabio@brc.ubc.ca*
Zoe White, Marine Theret, Nadia Milad, Fabio Rossi and Pascal Bernatchez shared co-authorship.

Introduction

Muscular dystrophies (MD) are a group of degenerative muscle wasting disorders that differ clinically with respect to age of onset, muscle groups affected, disease severity and overall lethality.[1] Duchenne MD (DMD) is the most common and severe form of MD and, similarly to the less severe Becker MD (BMD), is caused by abnormally low dystrophin (Dystro) expression or activity.[2] DMD boys experience progressive skeletal muscle wasting, loss of ambulation and early death if unmedicated due to cardiorespiratory comorbidities.[3,4] In contrast, the less severe and non-lethal limb-girdle MD type 2B (LGMD2B) results from mutations to the dysferlin (Dysf) gene.[5] Unlike DMD, LGMD2B does not interfere with normal cardiac or respiratory functions but does contribute to skeletal muscle degeneration later in life and independently of gender.[6] At the cellular level, Dystro-deficient muscles show abnormal calcium homeostasis, which increases sarcolemmal fragility and renders muscle fibres more susceptible to contraction-induced injury,[7] whereas Dysf-deficient myofibres show abnormal calcium-dependent sarcolemmal repair after injury due to blunted fusion of lipid patches to the muscle membrane.[8] Resultant cycles of myonecrosis and compensatory regeneration lead to the deposition of collagen-rich or lipid-rich infiltrates in the muscles of DMD or LGMD2B patients, respectively,[3,4] when regenerative potential is exhausted.[9] This is in stark contrast with rodent models of MD that show only mild skeletal or cardiac muscle phenotypes or fibro-fatty infiltration,[10] which has hampered the development of effective cures.

We have recently demonstrated that both Dystro-deficient and Dysf-deficient mice display human-like muscle wasting and severe ambulatory dysfunction following inactivation of their apolipoprotein E (ApoE) gene,[11,12] which is essential for normal lipid clearance, adipose tissue metabolism, inflammation and neurological homeostasis.[13] These mice displayed heightened levels of atherogenic plasma lipoproteins that correlated with the accelerated replacement of muscle fibres with non-functional fat-rich or collagen-rich infiltrates in MD-specific muscles, particularly when fed a high-fat diet (HFD).[11,12] In addition, we have recently reported a high prevalence of plasma lipid-related abnormalities in DMD and BMD patients including elevated plasma total cholesterol (TC) and triglyceride (TG) lipid fractions.[14] Dyslipidaemia was also observed in unmedicated DMD and carrier canine samples, indicating a primary state of dyslipidaemia even in the absence of muscle wasting.[14] These data suggest that loss of Dystro expression causes profound defects in lipoprotein handling, although the root cause of this phenomenon and whether dyslipidaemia plays an exacerbating role in muscle wasting are not known.

Herein, we show that the NPC1L1 cholesterol absorption blocker ezetimibe, a clinically approved cholesterol-lowering agent with few pleiotropic effects, can rescue ambulatory function and reduce muscle wasting and fibro-fatty infiltration in humanized models of LGMD2B and DMD while leaving non-MD-affected muscles unaffected. We further stress the role of cholesterol in MD-mediated disease pathology by reporting that directly raising dietary cholesterol and downstream circulating plasma low-density lipoprotein-associated cholesterol (LDL-C) results in drastically accelerated muscle wasting, inflammation and fibro-fatty accumulation, leading to poorer functional outcomes and reduced survival. Genetic analyses combined with mechanical and direct cholesterol injury assays reveal that excess cholesterol compromises sarcolemmal integrity and enhances macrophage recruitment, pathogenic cytokine signalling and extracellular matrix (ECM) remodelling. Together, our data suggest that cholesterol is a direct mediator of skeletal muscle damage in two different models of MD. The high prevalence of dyslipidaemia in MD populations likely exacerbates muscle pathology and if properly treated could delay the loss of muscle mass and ambulation or death.

Methods

Animal models and husbandry

All animals were housed in a 12 h/12 h light/dark cycle, temperature-regulated facility. All animal procedures were carried out in accordance with the guidelines and regulations set by the University of British Columbia (UBC), Animal Care Committee, and the UBC Animal Ethics Committee, Vancouver, BC. Experimental, LGMD2B (Dysf-null and Dysf/ApoE double knock-out) and DMD (*mdx* and *mdx*/ApoE double knock out) mice were generated by crossing either the Dysf-null B6.129-*Dysf* ^{tm1Kcam}, or Dystro-deficient B6Ros.Cg-*Dmd* $^{mdx\text{-}4Cv}$/J mice, with the ApoE-null B6.129P2-*Apoe* ^{tm1Unc}/J mice as previously described.[12,15] Experimental wild-type (WT) and ApoE-Null mice were generated by crossing C57BL/6J mice with ApoE-null B6.129P2-*Apoe* ^{tm1Unc}/J mice as previously described.[12,15] Mice were genotyped using the extraction protocols and primer sequences described in Sellers *et al*.[12]

Diets and drug treatment

Mice were supplemented *ad libitum* with the following diets at 2 months of age, where specified: regular chow (CHOW; LabDiet 5001); high-fat diet (HFD; Envigo, TD.88137; 0.2% total cholesterol, 21% total fat and 34% sucrose by weight); modified LabDiet 5001 with 2% added cholesterol (CHOL; TestDiet; TD.0009393; chow-based with 2% added cholesterol, 13.1% total fat and 3.7% sucrose by weight). Dietary interventions were started at 2 months of age. Ezetimibe (Zetia) was activated in a 1:1 ratio of EtOH and added to drinking water at a 15 mg/kg/day dose (starting at 2 months of age), which was titrated based on body weight and water consumption (averaged per cage). Ezetimibe is a novel sterol-absorption inhibitor that blocks NPC1L1-mediated cholesterol absorption of both dietary and biliary origin at the apical brush border membrane of enterocytes.[16] For chronic ezetimibe studies, Dysf/ApoE mice were assessed at 11 months of age and *mdx*/ApoE at 7 months owing to differences in disease progression, severity, rates of functional and skeletal muscle decline, and potential cardiorespiratory dysfunction predominantly in severe *mdx*/ApoE mice.

Gait tracking and hindlimb width

Analysis of gait was completed from ink imprint of hind paws recorded on paper from mice traversing a 1.5 m distance. Step length was defined as the distance between two consecutive imprints from the same foot. Areas in which a mouse paused were not included, and the overall step length per mouse was averaged from three replicates. Zeros were given to any animal with loss of function leading to a complete inability to ambulate. Gross morphology of hindlimbs were studied from photographs of euthanized animals upon removal of the epidermis, where 'width' was defined as the distance of a line drawn from the anterior tibial crest to the most posterior point of the gastrocnemius.

Tissue processing, immunofluorescence and immunohistochemistry

Dysferlinopathic patients and mouse models exhibit characteristic fibro-fatty replacement in limb-girdle muscles including triceps, gastrocnemius and quadriceps,[12,17–19] with minor diaphragm involvement.[12,20] Triceps and gastrocnemius are two muscle groups affected by dystrophin-deficiency,[21–24] although early and progressive diaphragm fibrosis resulting in respiratory insufficiency is the leading cause of death in DMD.[25,26] As such, primary limb muscle including the quadriceps, gastrocnemius and triceps were among those primarily assessed for chronic LGMD2B studies, whereas triceps and gastrocnemius limb muscles and diaphragm were assessed for DMD.

Mice were sacrificed under terminal anaesthesia (5% v/v isoflurane, 2 L O_2) via cardiac puncture and perfused with warmed Krebs solution (118 mmol/L NaCl, 22.5 mmol/L $NaHCO_3$, 4 mmol/L KCl, 1.2 mmol/L NaH_2PO_4, 2 mmol/L $CaCl_2$, 2 mmol/L $MgCl_2$ and 11 mmol/L dextrose). Histological analysis was performed on isolated muscles fixed in 10% formalin for 24 h then transferred to 70% EtOH. All appendicular muscles were cut transversely across the mid-belly. Diaphragm segments were removed by cutting a ~1 cm coronal strip, bordering (but not including) the central tendon. All muscles were embedded in cross-section, sectioned at 5 μm and stained with Masson's trichrome as previously reported.[12,15] Fat area was quantified by manually tracing adipocyte containing regions (previously confirmed by perilipin staining[12]), muscle damage area was quantified by manually tracing areas of muscle necrosis and bulk inflammation,[12] and healthy myofibre area was quantified by subtracting both fat and damage areas from total muscle area. The percentage of collagen content/fibrosis was measured using a positive pixel count algorithm in Aperio ImageScope software using the following parameters: hue value of 0.66 and hue width of 0.25.[12] Slides were scanned using an Aperio digital slide scanner and analysed using Aperio ImageScope Software.

Where adipocytes could not be reliably determined, perilipin staining was performed on serial paraffin sections (5 μm) using immunofluorescence, and quantified as above. Briefly, sections were routinely deparaffinized and antigen retrieval performed in 10 mM of citrate buffer at 90°C for 10 min. Slides were then cooled, washed in phosphate-buffered saline (PBS), then incubated in a block solution containing 3% normal goat serum and 0.3% triton X-100 in PBS for 60 min at room temperature (RT), prior to incubation with perilipin (Sigma #P1873; 1:200) overnight at 4°C. Slides were then washed with PBS and incubated in block solution containing secondary antibody (Thermo Fisher #A-21245) for 2 h at RT. Following antibody incubation, 3 × 5 min PBS washes were performed, and sections were mounted with Vectashield mounting medium with DAPI (Vector Laboratories). Images were acquired at ×10 and ×20 magnifications using a Nikon Eclipse Ni microscope, equipped with a device camera (Nikon Digital Sight DS-U3) and operated via NIS software.

MAC2 positive macrophage staining was performed on paraffin sections (5 μm) using immunohistochemistry. Briefly, sections were routinely deparaffinized, antigen retrieval performed in 10 mM of citrate buffer until boiling for 10 min in the microwave and sections cooled at RT for 30 min. Slides were then washed in PBS and quenched in 3% H_2O_2 for 15 min at RT before being rewashed in PBS. Sections were then blocked in 10% normal goat serum in PBS for 1 h at RT, prior to incubation with anti-mouse Galectin-3/MAC-2 (Cedarlane; #CL8942AP; 1:3000) overnight at 4°C. Slides were then

washed with PBS and incubated in block solution containing a goat anti-rat secondary antibody (Vector Laboratories; #BA-400; 1:1000) for 30 min at RT. Following antibody incubation, 3 × 5 min PBS washes were performed, and VECTASTAIN ABC reagents (Vector Laboratories; #SK6100) applied to sections as per manufacturer instructions. Sections were then rinsed in PBS before and after ImmPACT DAB reagents (Vector Laboratories; #SK-4105) were added for 1–2 min. Nuclei were counterstained with Haematoxylin and cover-slipped. Slides were scanned using an Aperio digital slide scanner.

Analysis of plasma cholesterol and triglycerides

Plasma was collected in heparinized tubes via cardiac puncture of mice, spun down at 4000 RPM for 10 min at 4°C and stored at −80°C. Plasma lipid profiles were assessed using the Siemens Advia 1800 system (Providence Health Care, St Paul's Hospital, BC, Canada) TC, high-density lipoprotein cholesterol (HDL-C) and TG. Assays were performed following manufacturer's instructions as previously reported.[12,14,15] LDL-C was calculated using the standard formula: TC − HDL-C − (TG/2.2).

Mechanical and cholesterol muscle injury assays

Mechanical injury experiments were conducted on 8- to 14-week-old Dysf-null and Dysf/ApoE mice. Mice were supplemented *ad libitum* with either a CHOW (LabDiet 5001) or a modified LabDiet 5001 with 2% added cholesterol (CHOL: TestDiet; #0009393), the latter of which was introduced 2 weeks prior to injury in order to induce hypercholesterolemia. Where applicable, ezetimibe (Zetia) was activated in a 1:1 ratio of EtOH and added to drinking water at 15 mg/kg/day upon transfer to a CHOL diet. Dosages were titrated to body weight and the volume of water consumed per cage. Mechanical injury was performed using the micro-pin injury model detailed in Desguerre *et al*.,[27] which induces an array of local myofibres lesions shown to mimic chronic MD muscle damage. Initially, mice were anaesthetised with 2% isoflurane and the right hindlimb shaved and 70% ethanol applied. Micro-pins (150 μm in diameter) were sterilized and handled with clamped forceps, leaving a pin length of ~2 mm. Subsequently, 15 random punctures (perpendicular to the longitudinal axis) were made to the right tibialis anterior (TA) muscle daily, over 14 days (under routine restraint). Following 14 days of injury, muscles were left to recover and harvested on Day 17 (D17) under terminal anaesthesia. Prior to study commencement, this procedure was performed on a small subset of mice under the guidance of the UBC veterinarian. Experimental parameters with respect to restraint, anaesthesia, pain management and post-injury monitoring were assessed. Animals were monitored daily over the 14 days of micro-injury, with a focus on health scores, pain signs, limping, bruising/wounds to the needle site (either due to needling or self-trauma). Post-injury analgesics were deemed not necessary as no visible pain signs, limping, swelling or bruising to the injury site were observed. Moreover, body weight assessments conducted in Dysf/ApoE (N = 9) mice fed a CHOL diet prior to, and post micro-pin injury indicated no overall effects on animal wellbeing (Supporting Information, *Figure* S1A). Contralateral TA's served as a non-injured control. Following excision, TA muscles were cut transversely across the mid-belly. The superior portion was taken for gene expression profiling (RNA-seq), and the inferior was paraffin processed (as above) and stained with Masson's trichrome.

For the direct cholesterol injury assay, experiments were conducted on 8- to 12-week-old C57BL/6 and Dysf-null animals fed a CHOW diet (LabDiet 5001). Briefly, mice were anaesthetised with 3% isoflurane, the hindlimbs shaved and 70% ethanol applied. Water soluble cholesterol (SIGMA, #C4951) was dissolved in pre-warmed 0.9% saline. Thirty microlitres of 0.9% saline containing 0.2 mg of cholesterol was injected into the right TA. A 30 μL injection of 0.9% saline into the left TA served as a sham control. To minimize inflammatory cell infiltration and to assess the direct cytotoxicity of cholesterol to muscle fibres, muscles were harvested 24 h after injection. Following excision, TA muscles were cut transversely across the mid-belly, and both halves embedded cross-sectionally, paraffin processed and stained with Masson's trichrome (as above).

RNA extraction and gene expression profiling—RNA-seq

To isolate total RNA, TA muscles were placed in 1 mL of RNAsol (Sigma Aldrich) and homogenized using a tissue homogenizer (OMNI International). RNA was extracted after 10 min precipitation in isopropanol and resuspended in RNAse free water and RNase inhibitor (1:20; New England BioLabs, #M0314L). RNA integrity was tested as previously described in Soliman *et al*.[28] using the Agilent Bioanalyzer 2100. RNA libraries were prepared following the standard protocol for the TruSeq Stranded mRNA library kit (Illumina) on the Illumina Neoprep automated microfluidic library prep instrument. Paired end sequencing was performed on the Illumina NextSeq 500 using the High Output 150 cycle Kits.[28]

RNA-seq bioinformatics analysis

All computational analyses of RNA-seq data were performed in R (v 3.6.2). Genes with less than two counts per million in at least two samples were filtered out. Batch correction was applied using Combat-seq under the sva package (v 3.35.2)

to appropriate samples.[29] Filtered and batch-adjusted (if applicable) data were processed and analysed using DESeq2 (v 1.26.0).[30] This included count normalization, principal component analysis (PCA) and differential expression analysis. Heatmaps shown in *Figures* 6, S8 and S9 represent gene expression normalized by *Z*-score across samples. Hierarchical cluster analysis shown in *Figure* S9C was computed with complete-linkage clustering over Euclidean distance. Over representation analysis with Gene Ontology (GO) was performed using clusterProfiler (v 3.14.3) with all significant genes (adjusted P value < 0.05) considered.[31] Genes associated with "ECM remodelling", "inflammation", and "programmed cell death" were queried from annotations under "GO0030198", "GO0006954", and "GO0012501", respectively. Bars associated with top enriched GO terms shown in *Figures* 6E and S9E reflect log-transformed adjusted P values.[30,31] All P values were adjusted by Benjamini–Hochberg correction.

Fluorescence-activated cell sorting and analysis

For *ex vivo* flow analysis, TA muscles were harvested and fascia was removed. TA muscle were cut in small pieces and incubated for an hour at 37°C under agitation in Collagenase D (Millipore Sigma 11 088 882 001; 1.5 U/mL) and Dispase II (Millipore Sigma 04 942 078 001; 2.4 U/mL). The suspension was then diluted in FACS buffer (PBS 2% serum, 2 mM EDTA) and filtered through a 40 μm cell strainer. After centrifugation at 400 *g* for 7 min at 4°C, cells were first incubated with Fcblock (Ablab) for 20 min on ice and then incubated with various cocktails of antibodies against cell markers (*refer to the next section for the list of antibody cocktails*) for 20–30 min on ice. After incubation, cells were washed in FACS buffer, Hoechst 33342 (Sigma B2261) and propidium iodide (PI; Thermo Fisher) were added to the cell suspension. Samples were analysed using BD LSRII and flowJo software.

Immune cell cocktail

CD45-APCFire750 (Biolegend, clone 30-F11, 1:400), Ly6G-PerCPCy5.5 (Biolegend, clone1A8, 1:200), CD3e-PerCPCy5.5 (Biolegend, clone 145-2C11, 1:200), NK1.1-PerCPCy5.5 (Biolegend, clone PK136, 1:200), CD11b-BV605 (Biolegend, clone M1/70, 1:1000), F4/80-FITC (Ablab, Clone BM8, 1:400). Macrophages were considered as CD45 + Ly6G/CD3/NK1.1− and CD11b/F480+.

Fibroadipogenic progenitors and muscle stem cells cocktail

CD45-APCFire750 (Biolegend, clone 30-F11, 1:400), CD31-APC (Ablab, clone 390, 1:500), a7integrin-FITC (Ablab, clone R2F2, 1:1000), Sca1-PeCy7 (Invitrogen, Clone D7 1:4000), VCAM-Biotin (Ablab, Clone MK1.9, 1:3000) and Streptavidin-PE (Ablab, 1:400). Fibroadipogenic progenitors (FAPs) were considered as CD45/CD31/a7int− Sca1+. Stem cells (SC) were considered as CD45/CD31/Sca1− a7int/VCAM+. Gating strategies for macrophage and progenitor populations are included in *Figure* S1B.

Statistical analyses

Statistical analyses were performed using GraphPad Prism 6. Statistical tests are specified in figure legends. Figures show data as mean plus standard error of the mean (SEM) and the number of animals used for each data set are specified in figure legends. Results with P values of less than 0.05 were considered statistically significant.

Data availability

Bulk RNA sequencing data sets generated during the current study are available. Software used to analyse the data is either freely or commercially available.

Results

The exacerbating role of these lipoprotein abnormalities in MD-associated muscle wasting was evaluated with the NPC1L1 blocker ezetimibe, an intestinal cholesterol absorption inhibitor with few pleiotropic effects. Treatment with ezetimibe of 2-month-old severe Dysf-deficient mice mimicking human LGMD2B pathology fully prevented ambulatory dysfunction (0% incidence vs. 33% for vehicle treatment; $P < 0.05$) (*Figure* 1A), completely rescued the 45% loss in step length (*Figure* 1B) and led to increased gross hindlimb muscle width when assessed at 11 months of age (*Figure* 1C). In severe *mdx* mice, ezetimibe had no effect on functional step length (*Figure* 1D) but increased hindlimb width (32%) and improved muscle morphology when assessed at 7 months of age (*Figure* 1E). Histological analyses using Masson's trichrome staining also revealed that ezetimibe significantly reduced fat accumulation in severe Dysf-deficient triceps, gastrocnemius and quadriceps (rectus femoris) muscles by 84%, 78% and 65%, respectively (*Figure* 2A–2B) compared with vehicle treatment, and contributed to a 34%, 113% and 44% increase in healthy myofibre area, respectively (*Figure* 2A–2B). In severe *mdx* mice lacking ApoE, ezetimibe treatment attenuated DMD-associated collagen infiltration in both triceps and gastrocnemius muscles by 56% and 63%, respectively (*Figure* 3A–3B *blue colour*), contributing to a 90% and 108% increase in total healthy myofibre area, respectively (*Figure* 3A–3B), although diaphragm pathology

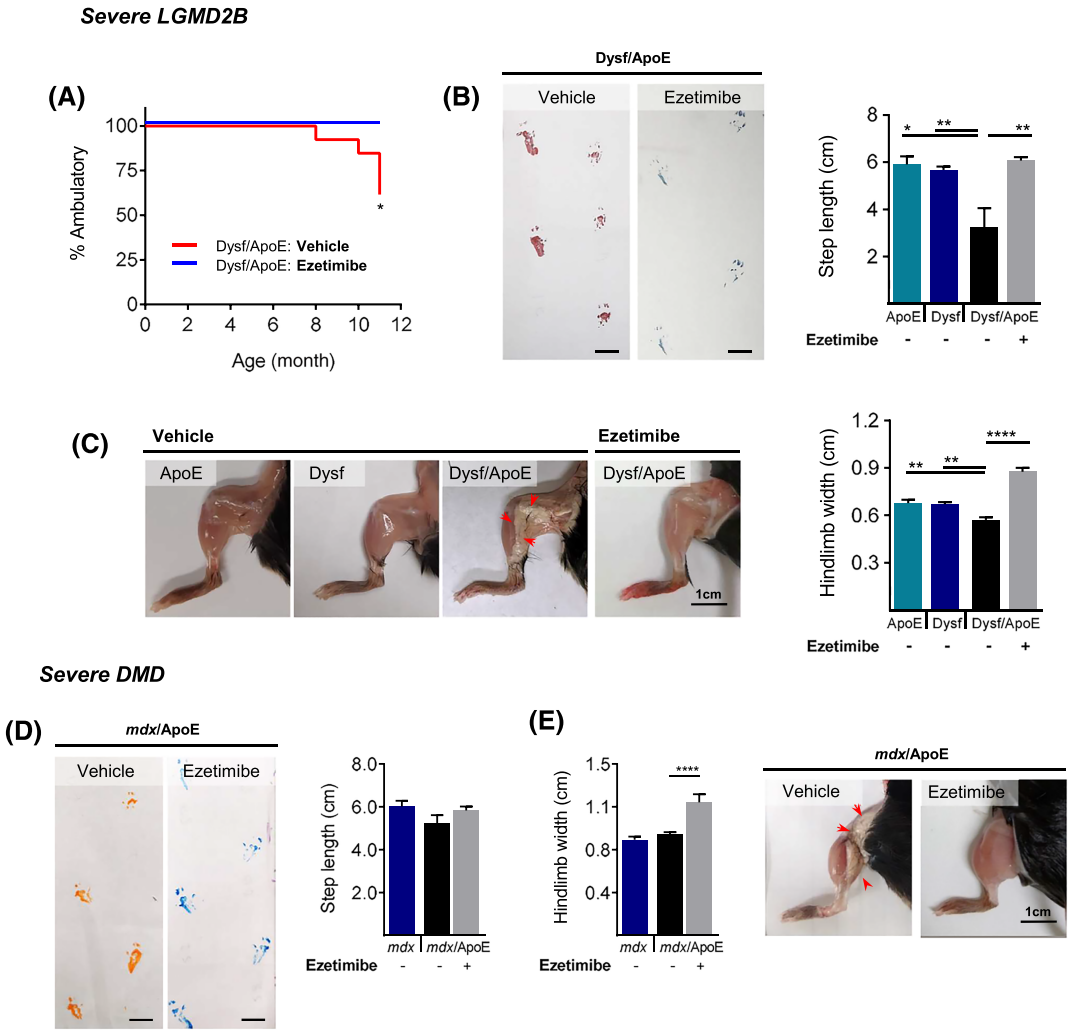

Figure 1 Ezetimibe preserves ambulatory function and prevents hindlimb muscle atrophy in severe mouse models of LGMD2B and DMD: (*A*) Kaplan–Meier curves demonstrating the percentage ambulation in Dysf/ApoE mice fed a HFD, with and without ezetimibe treatment; Mantel–Cox test; ($P < 0.05$). (*B*) Quantification of step length in vehicle ApoE, Dysf and Dysf/ApoE mice, and ezetimibe-treated Dysf/ApoE mice, and select representative images (fed a HFD, aged 11 months); a one-way ANOVA with Tukey's post-hoc test was used to compare means between vehicle cohorts. Comparisons between vehicle and treated Dysf/ApoE mice were compared by unpaired *t*-test. (*C*) Representative hindlimb images and respective quantification from vehicle ApoE, Dysf and Dysf/ApoE mice, and ezetimibe-treated Dysf/ApoE mice fed a HFD (aged 11 months); a one-way ANOVA with Tukey's post-hoc test was used to compare means between vehicle cohorts; comparisons between vehicle and treated Dysf/ApoE mice were compared by unpaired *t*-test. Arrows indicate areas of visible fibroadipogenic infiltration and facial thickening. (*D*) Representative images and quantification of step length in vehicle *mdx* and *mdx*/ApoE mice, and ezetimibe-treated *mdx*/ApoE mice fed a HFD (aged 7 months). Comparisons between both vehicle *mdx* and *mdx*/ApoE mice, and vehicle-treated *mdx*/ApoE mice were compared by unpaired *t*-test (*no significance*). (*E*) Representative images and quantification of hindlimb width of vehicle *mdx* and *mdx*/ApoE mice, and ezetimibe-treated *mdx*/ApoE mice fed a HFD (aged 7 months); unpaired *t*-test; arrows indicate areas of visible fibroadipogenic infiltration. N = 6–16 for Dysf/ApoE and N = 4–10 for *mdx*/ApoE cohorts. Mean ± SEM. $P < 0.05$ (*), $P < 0.01$ (**), $P < 0.001$ (***). Scale bars: 1 cm.

was not improved by ezetimibe (*Figure* 3A–3B). Improved skeletal muscle histology in severe LGMD2B and DMD mice was associated with reduced levels of total plasma cholesterol (TC; −44% and −61%, respectively) and LDL-C associated lipid fractions (LDL-C; −47% and −63%, respectively) (*Tables* S1 and S2; $P < 0.01$). Conversely, HDL-C and plasma TG were not significantly affected by ezetimibe in either model (*Tables* S1 and S2). No effect of NPC1L1-blockade was observed in triceps or gastrocnemius muscles from normolipidemic, Dysf-deficient (*Figures* S2–S3) or the triceps, gastrocnemius and diaphragms of *mdx* mice (*Figures* S4–S6), despite a significant reduction in plasma TC, LDL-C and HDL-C (*Tables* S1 and S2).

The exacerbating role of cholesterol in MD was further investigated by substituting the standard 0.2% cholesterol-containing HFD with a custom high 2% cholesterol chow-based diet (CHOL) from 2 months of age, which resulted in the early euthanasia of 100% of severe LGMD2B

DOI: 10.1002/jcsm.12879

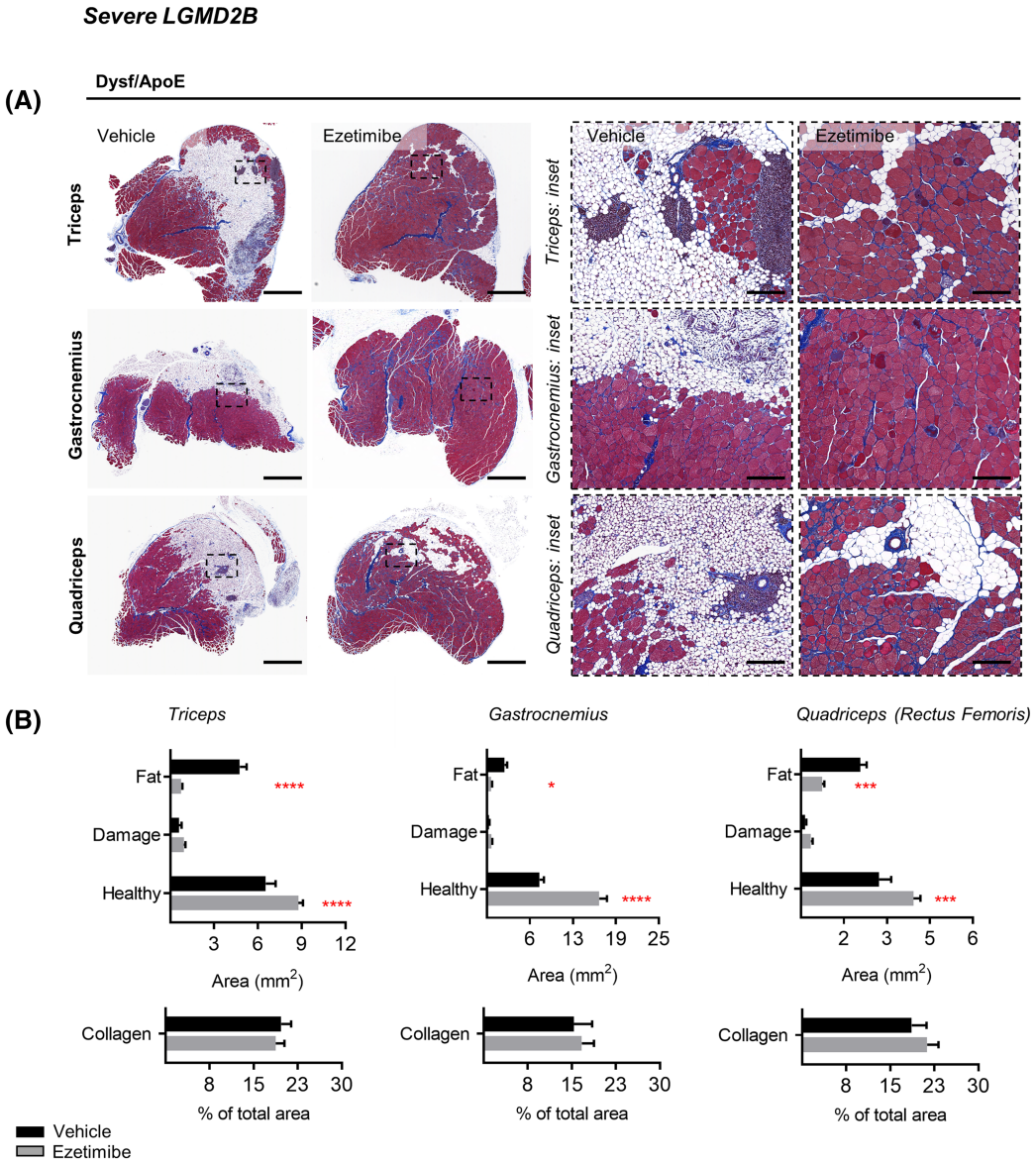

Figure 2 Ezetimibe prevents fat accumulation and collagen deposition in triceps, gastrocnemius and quadriceps muscles from severe LGMD2B mice. (*A*) Representative images of triceps, gastrocnemius and quadriceps muscles from vehicle-treated and ezetimibe-treated Dysf/ApoE (11 months) mice fed a HFD. Scale 1 mm for whole muscle images and 100 μm for insets. (*B*) Quantification of fat, damaged, and healthy myofibre areas, and percentage of collagen infiltration in triceps, gastrocnemius and quadriceps (rectus femoris only) muscles from vehicle-treated and ezetimibe-treated Dysf/ApoE mice fed a HFD aged 11 months; a two-way ANOVA with Sidak's post-hoc test was used to compare means between vehicle-treated and ezetimibe-treated cohorts. N = 7–10. Mean ± SEM. $P < 0.05$ (*); $P < 0.001$ (***); $P < 0.0001$ (****).

mice (*Figure* 4A). Further analyses revealed extensive thickening of hindlimb fascia in CHOL-fed mice at 4 to 5 months of age (*Figure* 4B, *red arrows*), as well as a 765% increase in triceps muscle damage and 71% loss of healthy myofibre area (*Figure* 4C–4D). Robust macrophage staining (MAC-2; *Figure* 4C; *images only*), perilipin-positive fat accumulation (87%; *ns*) and collagen deposition (58%; *ns*) were also shown to increase in CHOL-fed triceps (*Figure* 4C–4D). Notably, these were associated with increased plasma TC, which was highly enriched in LDL-C, and present in levels approximately 247% higher than age-matched, HFD-fed mice (*Figure* 4E). Accelerated ambulatory dysfunction leading to humane euthanasia and thickening of hindlimb fascia was also observed in Dysf/ApoE mice relative to ApoE and Dysf-null controls fed a CHOL diet for the same duration (*Figure* S7A–S7B). Increased muscle damage and collagen deposition (31-fold and 6-fold increase), leading to a 65% reduction in overall healthy myofibre area was also observed in Dysf/ApoE

DOI: 10.1002/jcsm.12879

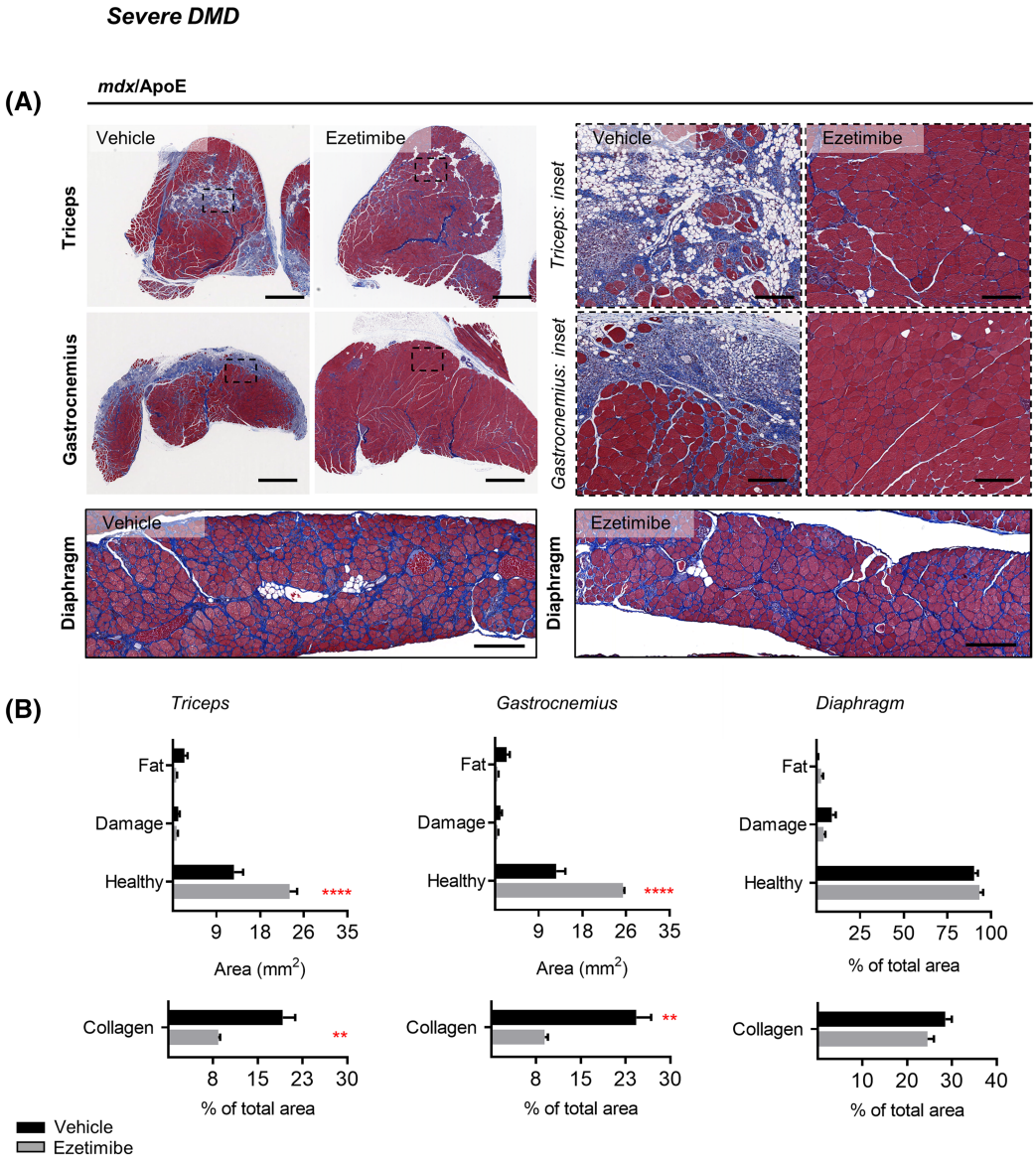

Figure 3 Ezetimibe prevents fat accumulation and collagen deposition in triceps and gastrocnemius muscles, but not the diaphragm in severe DMD mice. (*A*) Representative images of triceps, gastrocnemius and diaphragm muscles from vehicle-treated and ezetimibe-treated *mdx*/ApoE mice fed a HFD (aged 7 months). Scale 1 mm for whole muscle images and 100 μm for insets (200 μm for diaphragm). (*B*) Quantification of fat, damaged, and healthy myofibre areas, and percentage of collagen infiltration in triceps and gastrocnemius muscles from vehicle-treated and ezetimibe-treated *mdx*/ApoE mice fed a HFD. Due to section variability, diaphragm quantification was expressed as a percentage of total area for all parameters; a two-way ANOVA with Sidak's post-hoc test was used to compare means between vehicle-treated and ezetimibe-treated cohorts. N = 4–11. Mean ± SEM. $P < 0.01$ (**); $P < 0.0001$ (****).

triceps muscles relative to healthy controls (*Figure* S7C). This was again associated with an increase in LDL-C laden plasma cholesterol (reaching up to 47 mmol/L), and exceeding that of ApoE-null mice by 156% (*Figure* S7D).

In severe *mdx* mice, CHOL-feeding induced severe muscle atrophy in both triceps and gastrocnemius muscle groups, by reducing healthy myofibre area (−49% and −58%, respectively), compared with HFD-fed mice (aged 4 months; *Figure* 5A–5B). In gastrocnemius, a 92% increase in collagen deposition was also observed (*Figure* 5A–5B). Unlike Dysf/ApoE mice, severe *mdx* animals showed no plasma TC nor LDL-C elevation by CHOL when compared with HFD and instead presented with decreased levels of HDL-C (−80%; *ns*) and TG (−68%) (*Table* S3), a clear sign of plasma lipid handling differences between LGMD2B and DMD. Interestingly, *mdx*/ApoE mice fed a CHOL diet until 9 months experienced severe ambulatory dysfunction (refer to *Video* S1), in association with vast fibro-fatty infiltrates expanding up to 71% of triceps and 73% of gastrocnemius muscles (*Figure* 5A, blue, *images only*).

DOI: 10.1002/jcsm.12879

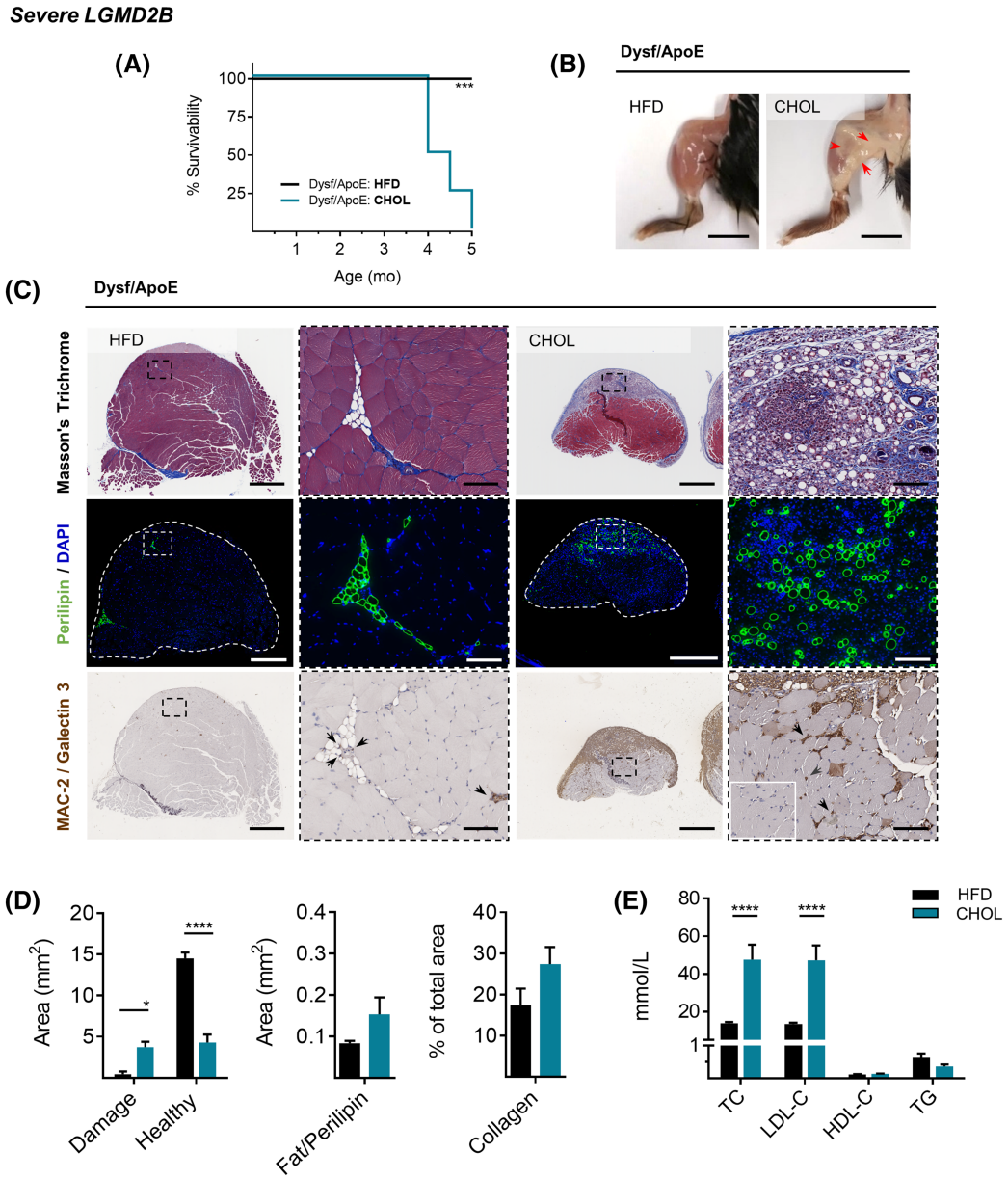

Figure 4 Severe LGMD2B mice fed a high 2% cholesterol diet (CHOL) display accelerated functional decline and worsened muscle damage compared to those fed a standard 0.2% cholesterol-containing HFD. (*A*) Kaplan–Meier curves comparing the percentage of CHOL and HFD-fed Dysf/ApoE mice requiring euthanization; Mantel–Cox test. $P < 0.001$ (***). (*B*) Representative hindlimb images from Dysf/ApoE mice fed either a CHOL or HFD, aged 4–5 months. Arrows indicate areas of visible fibroadipogenic infiltration. (*C*) Representative images of triceps muscles from CHOL-fed and HFD-fed Dysf/ApoE mice (aged 4–5 months) stained with Masson's trichrome, Perilipin and MAC2. No primary control for MAC2 staining embedded in inset. Scale 1 mm for whole muscle images and 100 μm for insets. (*D*) Quantification of damaged and healthy myofibre areas, perilipin/fat positive area and the percentage of collagen infiltration in triceps muscles from CHOL-fed and HFD-fed Dysf/ApoE aged 4–5 months; mean ± SEM; a two-way ANOVA with Sidak's post-hoc tests or unpaired *t*-test was used to compare means between cohorts. $P < 0.05$ (*); $P < 0.0001$ (****). (*E*) Plasma total cholesterol (TC), low-density lipoprotein (LDL-C), high-density lipoprotein (HDL-C) and triglyceride (TG) levels in Dysf/ApoE mice fed either a CHOL or HFD, aged 4–5 months; mean ± SEM; a two-way ANOVA with Sidak's post-hoc test was used to compare means between untreated cohorts. Mean ± SEM; $P < 0.0001$ (****). N = 4–5 mice per cohort for all measures.

To gain molecular insight into the deleterious role of cholesterol in MD-associated muscle wasting, severe LGMD2B mice were subjected to micro-pin-induced mechanical injury followed by histological, RNA-seq and FACS analyses. Increased muscle damage (425%) and collagen deposition (52%) were observed in injured-CHOL compared with injured-Chow muscles, and ezetimibe treatment completely mitigated this effect (*Figure* 6A). Similarly, RNA-seq analysis

DOI: 10.1002/jcsm.12879

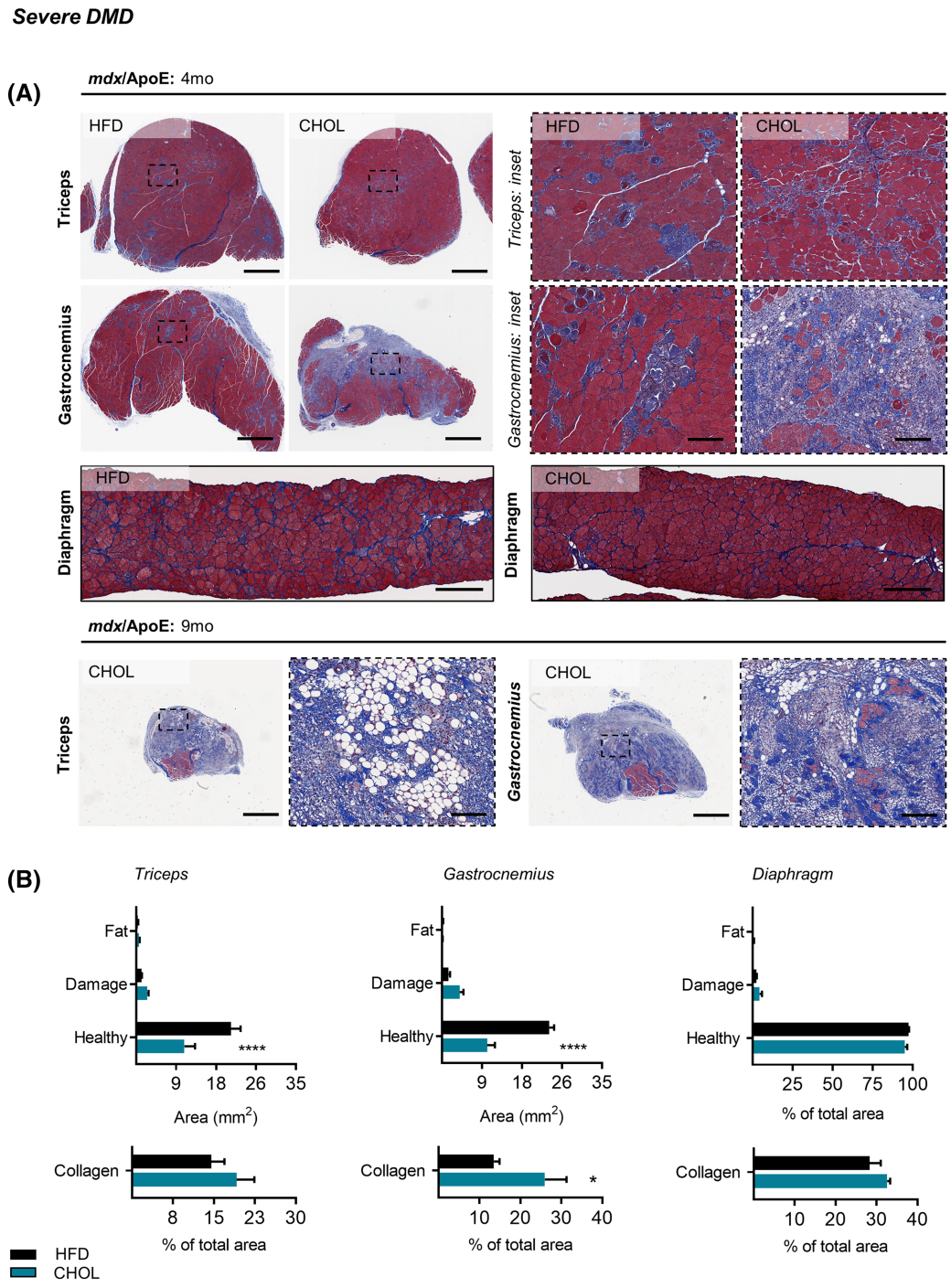

Figure 5 Severe *mdx* mice fed a CHOL diet display accelerated muscle damage compared with those fed a standard HFD. (*A*) Representative images of triceps, gastrocnemius and diaphragm muscles from severe *mdx* mice fed either a CHOL or HFD (aged 4 months) stained with Masson's trichrome, and representative images of triceps muscles from severe *mdx* mice fed a CHOL diet (aged 9 months) stained with Masson's trichrome. Scale 1 mm for whole muscle images and 100 μm for insets (100 μm for diaphragm). (*B*) Quantification of fat, damaged, and healthy myofibre areas, and percentage of collagen infiltration in triceps and gastrocnemius muscles from CHOL-fed and HFD-fed *mdx*/ApoE mice aged 4 months. Due to section variability, diaphragm quantification was expressed as a percentage of total area for all parameters; a two-way ANOVA with Sidak's post-hoc test or unpaired *t*-test was to compare means between cohorts. Mean ± SEM; $P < 0.05$ (*); $P < 0.0001$ (****). $N = 4–5$. Quantification was not performed for the 9 month subset of animals due to early euthanasia to assure humane endpoint ($N = 2$).

DOI: 10.1002/jcsm.12879

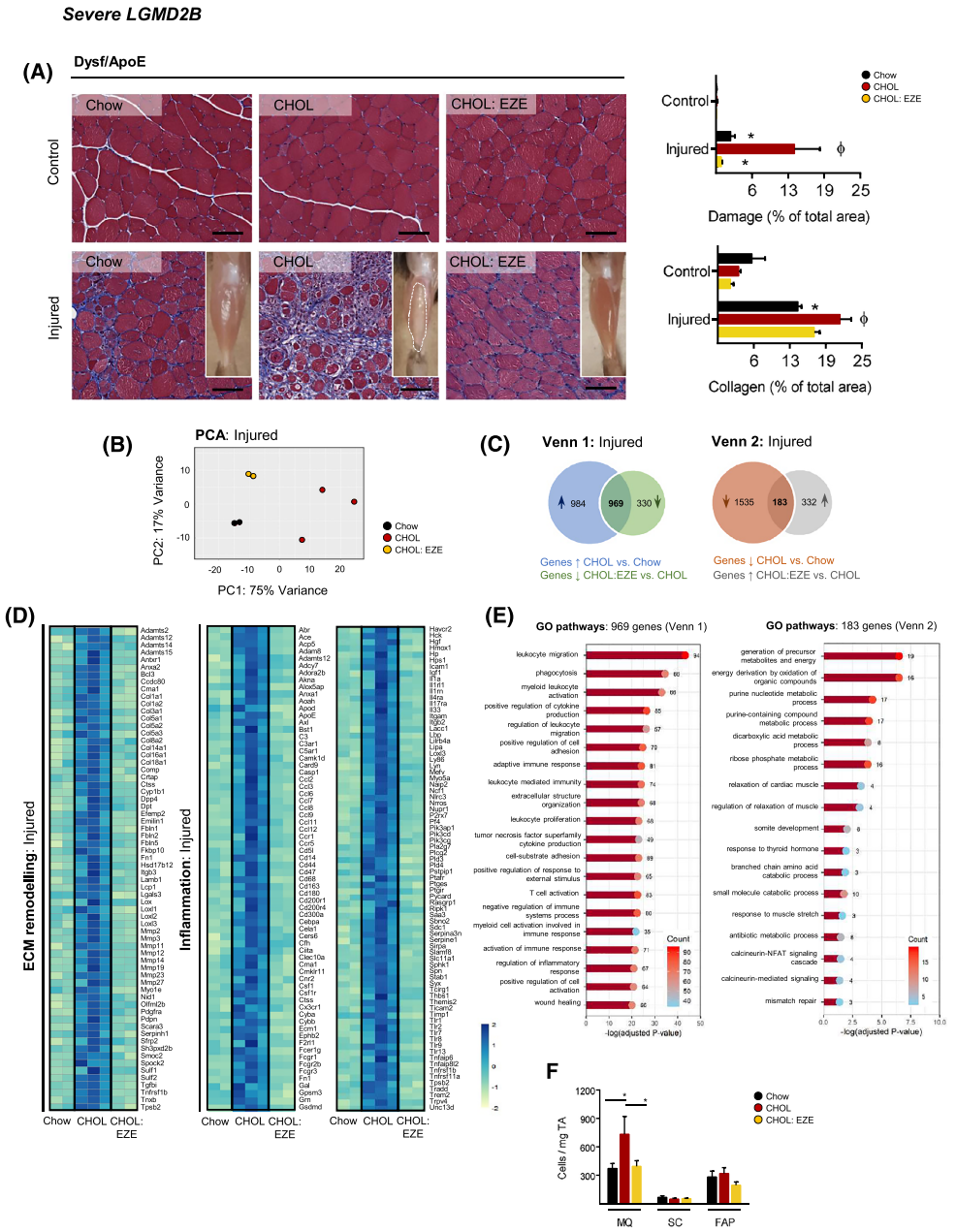

Figure 6 Ezetimibe mitigates skeletal muscle damage, ECM-remodelling and inflammatory signalling following mechanically induced injury in severe LGMD2B mice fed a CHOL diet. (*A*) Representative images and quantification in uninjured-control and mechanically injured TA muscles from severe LGMD2B mice fed either regular chow (Chow), CHOL or a CHOL diet with ezetimibe (CHOL:EZE). Scale 150 μm. *N* = 4–7 mice per cohort. Insets: representative images of gross TA morphology, and outline indicates macroscopic injury. Quantification of total muscle damage and collagen deposition (as a percentage of total TA area) in control and injured TA muscles of severe LGMD2B mice fed Chow, CHOL or CHOL:EZE; a two-way ANOVA with Sidak's post-hoc tests was used to compare means between injured cohorts. Asterisk (*) indicates significantly different from CHOL-injured; $P < 0.05$ (*). A two-way ANOVA with Tukey's post-hoc tests was used to compare means between control and injured cohorts; $P < 0.05$ (ϕ). *N* = 4–7 mice per cohort. (*B*) Principal component analysis (PCA) of global gene expression in injured muscles of severe LGMD2B mice in Chow, CHOL and CHOL:EZE cohorts. *N* = 2–3 mice. (*C*) Venn diagrams from RNA-seq experiments indicating the number of genes differentially up-regulated in CHOL vs. Chow and down-regulated in CHOL:EZE vs CHOL (Venn 1), and the number of genes differentially down-regulated in CHOL vs. Chow and up-regulated in CHOL:EZE vs. CHOL (Venn 2). *N* = 2–3 mice. (*D*) Heat maps of relative ECM remodelling and inflammatory gene expression in mechanically injured TA muscles from severe LGMD2B mice fed Chow, CHOL or CHOL:EZE. *N* = 2–3 mice. (*E*) Gene Ontology analysis of the 969 and 183 differentially expressed genes (DEGs) represented in Venn 1 and Venn 2. *N* = 2–3 mice. (*F*) Quantification of CD45 + Ly6G/CD3/NK1.1−, CD11b/F480+ macrophages (MQ), CD45/CD31/Sca1− a7int/VCAM+ muscle stem cells (SC) and CD45/CD31/a7int− Sca1+ fibroadipogenic progenitors (FAP). A two-way ANOVA with Tukey's post-hoc tests was used to compare means between control and injured cohorts; $P < 0.05$ (*); *N* = 5–10 mice per cohort. Mean ± SEM.

showed clear PCA plot separation (covering 75% variance) between injured-Chow and injured-CHOL muscles (*Figure* 6B), whereas greater similarity was observed between injured-Chow and injured-CHOL:EZE cohorts (17% variance) (*Figure* 6B). Further transcriptomic analysis revealed 3671 DEGs between injured-CHOL and injured-Chow muscles (1953 up-regulated and 1718 down-regulated; *Figure* 6C). Ezetimibe reversed the expression of 969 of the 1953 genes up-regulated by CHOL and injury (Venn 1) and reversed the expression of 183 of the 1718 genes down-regulated by CHOL and injury (Venn 2) (*Figure* 6C). Heat maps and GO pathway analysis of the 969 up-regulated genes counter-regulated by ezetimibe (Venn 1) showed that transcripts associated with ECM remodelling, inflammation (*Figure* 6D–6E) and programmed cell death (*Figure* S8A) were significantly affected by both CHOL and EZE. Comparatively, GO pathway analysis of the 183 down-regulated genes counter-regulated by ezetimibe (Venn 2) showed that pathways associated muscle metabolic processes were among the most affected (*Figure* 6E). Consistent with an elevated inflammatory transcriptome, FACS analyses revealed increased macrophage populations in injured-CHOL compared with injured-Chow muscles (98%); an effect prevented in injured-CHOL:EZE muscles (*Figure* 6F). Interestingly, neither diet nor ezetimibe affected SC or FAP cell populations following injury (*Figure* 6F). Hence, ezetimibe inhibits inflammation and ECM remodelling in LGMD2B-prone muscles, resulting in lower macrophage recruitment and thus attenuated damage in already fragilized myofibres.

Increased muscle damage and collagen deposition was also observed in injured-Dysf/ApoE mice relative to injured-ApoE and Dysf controls fed a CHOL diet (*Figure* S9A). Transcriptomic analysis of skeletal muscles across the three cohorts indicated that CHOL-injured ApoE and Dysf/ApoE samples shared much higher similarity than CHOL-injured Dysf samples, as shown by PCA and hierarchical clustering of all significant DEGs (*Figure* S9B–S9C). Complimentary gene sets associated with ECM remodelling, inflammation and programmed cell death were also more expressed in CHOL-injured ApoE and Dysf/ApoE, than Dysf samples (*Figures* S8B and S9D). To further assess the transcriptomic differences between CHOL-injured ApoE and Dysf/ApoE samples, we performed GO pathway analysis of all up-regulated and down-regulated DEGs between the two groups (*Figure* S9E–S9F). We observed pathways associated with ECM organization and leukocyte migration to be the most enriched in CHOL-injured Dysf/ApoE samples, and again suggesting a more severe and cholesterol-dependent injury response relative to injured-ApoE samples.

Finally, the susceptibility of LGMD2B-affected muscles to cholesterol-mediated damage was also tested in normolipidemic WT and Dysf-deficient mice subjected to direct intramuscular cholesterol injection. Interestingly, Dysf-deficient myofibres were more susceptible to cholesterol-induced toxicity 24 h post-injection, resulting in 122% more muscle damage than WT muscles (*Figure* S10A).

Discussion

The current study shows that inhibition of cholesterol absorption with the NPC1L1 inhibitor ezetimibe prevents ambulatory dysfunction and drastically reduces MD-specific muscle pathologies including the adipogenic-rich muscle deposition of LGMD2B (triceps, gastrocnemius and quadriceps), and the fibrogenic-rich infiltration characteristic of DMD (triceps and gastrocnemius) observed in severe MD mouse models caused by ApoE gene inactivation. This is likely a result of attenuated cholesterol-induced damage of fragilized myofibres and the suppression of inflammatory cytokine signalling, pathogenic ECM remodelling and macrophage recruitment. The exacerbating role of cholesterol in MD-associated muscle wasting was further supported by the deleterious effects of a cholesterol-rich diet and direct cholesterol injection-induced damage in MD-affected muscles, and the lack of therapeutic effect of ezetimibe in MD mice with normal ApoE expression and therefore low LDL-C levels. Having recently shown that DMD patients are afflicted by a new type of genetic dyslipidaemia, the current study suggests that the primary dyslipidaemic state in DMD could play an active part in the progressive muscle wasting process observed clinically. Hence, treatment of MD patients with ezetimibe could attenuate the rate of muscle function decline, delay ambulatory dysfunction and death. The data presented herein support the concept that lipometabolic comorbidities could play a potential role in LGMD2B and DMD muscle pathologies.

While our data depict a direct toxic effect of cholesterol in MD muscles, cholesterol is nonetheless essential to cellular homeostasis. Physiological levels of membrane cholesterol are critical for the preservation of plasmalemmal and sarcolemmal fluidity and rigidity, and help provide a physical template to the signalling processes found in specialized lipid microdomains.[32] However, whether an increase in global myofibre cholesterol exposure or a change in its origin (endogenously synthesized vs. plasma-derived cholesterol) exacerbate the cellular manifestations of MD is unknown. Indeed, an increase in muscle cholesterol levels could create a toxic state of 'cholesterol overload' or instead promote a compensatory down-regulation of endogenously synthesized cholesterol from mevalonate/HMGCoA reductase-derived pathways, either of which could be deleterious to skeletal muscle health. Exactly how the loss of functional dysferlin or dystrophin affects this homeostatic process is unknown, particularly as skeletal muscles typically synthesize little *de novo* cholesterol,[33,34] implying a significant uptake of cholesterol from extracellular sources. While we show that direct extracellular cholesterol injection causes rapid muscle damage in MD models, the muscle-specific deletion of HMGCoA

reductase (HMGCR), and thus endogenous cholesterol synthesis, also causes severe skeletal muscle atrophy and can contribute to increased rates of myonecrosis.[35] This suggests that any disruption to muscle cholesterol levels could alter sarcolemmal integrity making it more susceptible to physical stress, blunt sarcolemmal repair, or dysregulate intracellular calcium homeostasis or extracellular matrices.[36] Further studies will be needed to characterize the role cholesterol synthesis and uptake play in myofibre integrity.

In addition to blunted cholesterol tolerance in MD, our data reveal a cholesterol-mediated up-regulation of pathogenic ECM, inflammatory and programmed cell death-associated transcripts, and heightened macrophage infiltration (as well as their down-regulation with ezetimibe), providing a mechanistic whole-tissue snapshot of the chronic effect cholesterol has on MD muscle wasting. Indeed, dysferlin-deficient muscle fibres are already known to exhibit dysregulated lipometabolic gene expression and the enrichment of phospholipids, sphingolipids and cholesterol species within the skeletal muscle lipidome as well as inherent sarcolemmal phospholipid abnormalities.[37] In light of our studies, cholesterol induces primary MD sarcolemmal disturbances that precede macrophage infiltration and cytokine up-regulation. Despite an observable acceleration of fibrogenic signalling pathways, FAPs were not up-regulated following injury as previously shown,[38] likely owing to the chronic nature of the damage model.[27] Notably however, ECM transcripts modulated by both CHOL and ezetimibe treatment included ADAMTS (a disintegrin and metalloproteinase with thrombospondin motifs), MMPs (matrix metalloproteinases), TIMPs (tissue inhibitor of MMP), and collagens, which can also be secreted by macrophages and modulated by their inflammatory mediators, as observed in wound healing studies.[39] MAC-2/Galectin-3 positive macrophages with a more M2-like phenotype are also typical of early, cholesterol-driven atherosclerotic lesions.[41] However, the interplay between cells in the skeletal muscle milieu is likely more complex than what is depicted in the current study and will thus require additional experiments with advanced transgenic markers of cell origin.

From a pharmacotherapeutic perspective however, whether other cholesterol-lowering medications will promote a greater level of myofibre integrity than ezetimibe remains to be determined. Indeed, treatment of *mdx* mice with the HMGCR inhibitor simvastatin was shown to ameliorate intramuscular inflammation and fibrosis and to improve functional skeletal muscle, diaphragm and cardiac parameters via anti-inflammatory and anti-oxidative pleiotropism rather than plasma LDL-C lowering.[42-44] However, it is likely that cholesterol and its specific source play a role in the muscle wasting process, as well as the level of dyslipidaemia in the model used—a critical parameter when using models of MD—as human MD patients are also dyslipidaemic.[14] Moreover, recent miRNA profiling of plasma from paediatric Duchenne patients has also highlighted the dysregulation of genes governing lipid metabolism and endogenous cholesterol synthesis, including sterol-regulatory binding proteins and downstream mevalonate pathway mediators, such as HMGCR.[42] The treatment of normal and dystrophic mice with rosuvastatin has been associated with accelerated muscle atrophy and heightened rates of inflammation and fibrosis in cardiac and skeletal muscle groups,[45] suggesting that inhibition of endogenous cholesterol synthesis is not as straightforward as expected. While some of these discrepancies may in part be explained by the complex activity and ubiquitous expression of HMGCR, the different pharmacokinetic profiles, dosages and lipophilicity of statins used, which can influence their efficacy,[46,47] the mechanism of action of ezetimibe is far simpler than that of statins; it is typically well tolerated in patients, with fewer adverse and/or pleotropic effects,[48-50] and its target NPC1L1 is far more restricted to enterocytes although humans express higher levels of hepatic NPC1L1 than mice,[16,51] and ezetimibe shows no anti-muscle wasting effects in MD mice expressing ApoE, further stressing a high LDL-C/non-HDL-C level-dependent effect. The lipid-altering effects of both endogenous cholesterol and cholesterol absorption inhibitors as either stand-alone monotherapies or in combination should be further investigated in MD.

It must be noted that our experiments in MD mice were performed in the absence of ApoE expression in an attempt to recapitulate the non-HDL-C-rich lipid profile observed in humans and particularly that of DMD patients, which is an important study limitation. Indeed, which lipoprotein fraction is most toxic to muscles and is being targeted by ezetimibe is at this point unknown; loss of ApoE switches the typical HDL-C-rich plasma lipid profile of mice to a profile highly enriched in chylomicrons and VLDL-C with a more moderate increase in LDL-C and IDL-C, whereas humans are rich in LDL-C, the main lipoprotein responsible for delivery of cholesterol to peripheral tissues. To further complexify the lipometabolic abnormalities in MD, our data also demonstrate significant lipid profile differences between severe LGMD2B and DMD mice fed a CHOL diet, which suggests that dysferlin and dystrophin have direct but diverging effects on plasma lipoprotein composition and metabolism. While there is no data on potential plasma lipid abnormalities in LGMD2B patients, DMD and BMD individuals display a higher prevalence of hypertriglyceridemia that could contribute to other lipoprotein irregularities including variations in HDL-C activity,[52] which can modulate intracellular glucose and mitochondrial homeostasis in skeletal muscle independently of its role in lipid transport.[53] Further, standard DMD patient care includes treatment with glucocorticosteroids and either ACE or angiotensin II inhibitors. Thus, whether lipid-lowering medications can be safely included in this range of medications remains to be tested. While very few studies have documented a therapeutic response in two highly heterogeneous types of MD, it must be noted that not all DMD and LGMD2B rodent muscle tissues are equally affected by high lipid environments.

Dysf-deficient and *mdx* triceps and gastrocnemius muscles show predictable lipid-induced exacerbation[11,12]; however, *mdx* quadriceps show little to no exacerbation compared with Dysf-deficient quadriceps.[11] More intriguing is the near-absence of lipid-induced exacerbation of *mdx* cardiac muscle[11] or diaphragm, which suggests that translating lipid-lowering approaches to patients may result in unexpected therapeutic effects that vary with the type of MD investigated.

In summary, our results reveal for the first time that NPC1L1 cholesterol absorption blockade drastically improves ambulation function and attenuates muscle wasting and fibro-fatty infiltration in severe LGMD2B and DMD mouse models with humanized skeletal muscle pathologies. More importantly, we provide evidence that cholesterol, particularly plasma-derived LDL-C, is a primary mediator of MD-associated skeletal muscle damage. In light of recent findings implicating plasma lipoprotein irregularities[14] and lipometabolic deficiencies[37] in MD, we suggest that ezetimibe may be a safe and effective therapeutic option for the long-term management of appendicular muscle wasting in patients with either dysferlin or dystrophin-deficient muscular dystrophies.

Acknowledgements

We would like to thank Tatjana Ponomarev and Lubos Bohunek (Centre for Heart and Lung Innovation, UBC) for their technical support for all animal experiments and Marie-Élaine Clavet for her help with MAC-2 staining. This work was supported from grants from the Canadian Institutes of Health Research and JAIN Foundation (PJT156060), Heart and Stroke Foundation of Canada G19-26513 and MITACS Accelerate Fellowship (P.B. and Z.W.). MT was supported by the Fondation pour la Recherche Medicale (FRM; 40248); by the European Molecular Biology Organization (EMBO; ALTF 115-2016), by the Association contre les myopathies (AFM; 22576), and by Michael Smith Foundation for Health Research (MSFHR; 18351). The authors of this manuscript certify that they comply with the ethical guidelines for authorship and publishing in the *Journal of Cachexia, Sarcopenia and Muscle*.

Online supplementary material

Additional supporting information may be found online in the Supporting Information section at the end of the article.

Figure S1. Body weight measurements and FACS gaiting strategies for LGMD2B micro-pin injury experiments. (A) Body weights of severe LGMD2B mice on a CHOL-diet, taken on day 1 (D1) of mechanical injury, and upon its completion (D17). *N* = 9. (B) FACS gating strategy for immune cells, endothelial cells (EC), Fibro-adipogenic progenitors (FAP) and myogenic muscle stem cells (SC) in severe LGMD2B mice subjected to mechanical-induced injury. Immune Cells: CD45+; EC: CD45- CD31+; FAPs: CD45/CD31/a7integrin- Sca1+; SC: CD45/CD31/Sca1- a7integrin/VCAM+

Figure S2. Ezetimibe has no effect on normolipidemic Dysf-deficient triceps muscles. (A) Representative images of triceps muscles from HFD-fed, vehicle and ezetimibe treated ApoE, Dysf and Dysf/ApoE mice (aged 11mo) stained with Masson's trichrome. Scale 1 mm for whole muscle images and 100 μm for insets. (B) Quantification of fat, damaged, and healthy myofiber areas, and percentage collagen infiltration in the triceps of vehicle and ezetimibe treated ApoE, Dysf and Dysf/ApoE fed a HFD (aged 11mo); a two way ANOVA with Sidak's post-hoc test was used to compare means between genotypes in each cohort; $P < 0.05$ (*); $P < 0.0001$ (****). A two-way ANOVA with Tukey's post-hoc tests were used for genotype comparisons between vehicle and Ezetimibe treated cohorts; $P < 0.05$ (ϕ), $P < 0.0001$ (ϕϕϕϕ). *N* = 4–8 for ApoE, *N* = 7–9 for Dysf and *N* = 6–9 for Dysf/ApoE cohorts; Mean±SEM.

Figure S3. Ezetimibe has no effect on normolipidemic Dysf-deficient gastrocnemius muscles. (A) Representative images of gastrocnemius muscles from HFD-fed, vehicle and ezetimibe treated ApoE, Dysf and Dysf/ApoE mice (aged 11mo) stained with Masson's trichrome. Scale 1 mm for whole muscle images and 100 μm for insets. (B) Quantification of fat, damaged, and healthy myofiber areas, and percentage of collagen infiltration in the gastrocnemius muscles of vehicle and ezetimibe treated ApoE, Dysf and Dysf/ApoE fed a HFD (aged 11mo); a two way ANOVA with Sidak's post-hoc test was used to compare means between genotypes in each cohort; $P < 0.01$ (**); $P < 0.001$ (***), $P < 0.0001$ (****). A two-way ANOVA with Tukey's post-hoc tests were used for genotype comparisons between vehicle and Ezetimibe treated cohorts; $P < 0.0001$ (ϕϕϕϕ). *N* = 3–7 for ApoE, *N* = 6–12 for Dysf and *N* = 7–9 for Dysf/ApoE cohorts; Mean±SEM.

Figure S4. Ezetimibe has no effect on normolipidemic Dystrophin-deficient *mdx* triceps muscles. (A) Representative images of triceps muscles from HFD-fed, vehicle and ezetimibe treated *mdx* and *mdx*/ApoE (aged 7mo) stained with Masson's trichrome. Scale 1 mm for whole muscle images and 100 μm for insets. (B) Quantification of fat, damage, and heathy myofiber areas and percentage collagen deposition in triceps muscles of vehicle and ezetimibe treated *mdx* and *mdx*/ApoE (aged 7mo); a two way ANOVA with Sidak's post-hoc test was used to compare means between cohorts. *N* = 6–9 for *mdx* and *N* = 4–7 for *mdx*/ApoE cohorts; Mean ±SEM; $P < 0.05$ (*); $P < 0.01$ (**); $P < 0.001$ (***); $P < 0.0001$ (****).

Figure S5. Ezetimibe has no effect on normolipidemic Dystrophin-deficient *mdx* gastrocnemius muscles. (A) Representative images of gastrocnemius muscles from HFD-fed, vehicle and ezetimibe treated *mdx* and *mdx*/ApoE mice (aged 7mo) stained with Masson's trichrome. Scale 1 mm for whole muscle images and 100 μm for insets. (B) Quantification of fat, damaged, and healthy myofiber areas, and percentage of collagen deposition in gastrocnemius muscles of vehicle and ezetimibe treated *mdx* and *mdx*/ApoE mice (7mo); a two way ANOVA with Sidak's post-hoc test was used to compare means between cohorts. N = 6–11 for *mdx* and N = 4–7 for *mdx*/ApoE cohorts; Mean±SEM; $P < 0.05$ (*); $P < 0.01$ (**); $P < 0.001$ (***); $P < 0.0001$ (****).

Figure S6. Ezetimibe has no effect on normolipidemic Dystrophin-deficient *mdx* diaphragm. (A) Representative images of the diaphragm from HFD-fed, vehicle and ezetimibe treated *mdx* and *mdx*/ApoE mice (aged 7mo) stained with Masson's trichrome. Scale 200 μm. (B) Quantification of fat, damage, heathy myofiber area and collagen deposition as a percentage of total muscle area in diaphragm of vehicle and ezetimibe treated *mdx* and *mdx*/ApoE mice (aged 7mo); a two way ANOVA with Sidak's post-hoc test was used to compare means between cohorts, no significance was detected. N = 6–9 for *mdx* and N = 4–7 for *mdx*/ApoE cohorts; Mean ±SEM.

Figure S7. Severe LGMD2B mice fed a CHOL diet display accelerated muscle damage compared to ApoE and Dysf controls. (A) Kaplan–Meier curves demonstrating the percentage survivability in ApoE, Dysf and Dysf/ApoE mice (aged 4-5mo) fed a CHOL diet; Mantel-Cox test; ($P < 0.001$). (B) Representative hind-limb in ApoE, Dysf and Dysf/ApoE mice (aged 4-5mo) fed a CHOL diet. (C) Representative images of triceps muscles from ApoE, Dysf and Dysf/ApoE mice fed a CHOL diet. Scale 1 mm for whole muscle images and 150 μm for insets. (D) Quantification of fat, damaged, and healthy myofiber areas, and percentage of collagen deposition in triceps of ApoE, Dysf and Dysf/ApoE mice fed a CHOL diet; a two way ANOVA with Sidak's post-hoc test was used to compare means between cohorts. $P < 0.05$ (*); $P < 0.01$ (**); $P < 0.0001$ (****). N = 3–7. (E) Plasma Total Cholesterol (TC), low density lipoprotein (LDL-C), high density lipoprotein (HDL-C) and triglyceride (TG) levels in ApoE, Dysf and Dysf/ApoE mice. a two way ANOVA with Sidak's post-hoc test was used to compare means between cohorts. Asterisk (*) indicates a significantly different from ApoE and Dysf genotypes; $P < 0.0001$ (****). Hash (#) indicates a significant difference between ApoE and Dysf; $P < 0.05$ (#). N = 4–5. Mean±SEM.

Figure S8. Heatmaps of relative programmed cell death-associated gene expression in mechanically-injured muscles from severe LGMD2B mice and ApoE and Dysf controls. (A) Relative gene expression in mechanically-injured TA muscles from severe LGMD2B mice fed Chow, CHOL or CHOL:EZE. N = 2–3 mice. (B) Relative gene expression in mechanically-injured TA muscles from control ApoE, Dysf and Dysf/ApoE mice fed CHOL. N = 2–3 mice.

Figure S9. Skeletal muscle damage, ECM-remodelling and inflammatory signalling following mechanically-induced injury in severe LGMD2B and control ApoE and Dysf mice fed a CHOL diet. (A) Representative images and quantification of total muscle damage and collagen deposition (as a percentage of total TA area) in uninjured-control and mechanically-injured TA muscles from ApoE, Dysf and Dysf/ApoE mice fed a CHOL diet. Scale 150 μm. A two way ANOVA with Sidak's post-hoc tests was used to compare means between injured cohorts. Asterisk (*) indicates significantly different from CHOL-injured ApoE and Dysf cohorts; $P < 0.05$ (*). A two way ANOVA with Tukey's post-hoc tests was used to compare means between control and injured cohorts; $P < 0.05$ (ϕ). N = 3–7. (B) Principal component analysis (PCA) and (C) hierarchical clustering of global gene expression in uninjured-control and mechanically-injured TA muscles from ApoE, Dysf and Dysf/ApoE mice fed a CHOL diet. N = 2–3 mice. (D) Heat maps of relative ECM remodeling and inflammatory gene expression in mechanically-injured TA muscles from ApoE, Dysf and Dysf/ApoE mice fed a CHOL diet. N = 2–3 mice. (E-F) GO pathway analysis and heat maps depicting the top 50 upregulated and downregulated DEGs between Dysf/ApoE and ApoE cohorts. N = 3. Mean±SEM.

Figure S10. Direct cholesterol injection exacerbates myofibers damage in dysferlin-deficient muscles (A) Representative images TA muscles from wild-type (WT) and Dysferlin-deficient (Dysf) mice 24 hours after either Saline (SHAM) or water soluble cholesterol injection, and quantification of muscle damage (as a percentage of total TA area) Scale 450 μm for whole muscle images and 100 μm for insets. A two way ANOVA with Tukey's post-hoc test was used for direct mean comparisons. Mean±SEM; $P < 0.01$ (**), $P < 0.001$ (***), $P < 0.0001$ (****). N = 5 for all groups.

Data S1. Supporting information

Table S1. Effect of ezetimibe on plasma lipoprotein and triglyceride concentrations in HFD-fed Dysf, ApoE and Dysf/ApoE mice at 11mo age.

Table S2. Effect of ezetimibe on plasma lipoprotein and triglyceride concentrations in HFD-fed mdx and mdx/ApoE mice at 7mo age.

Table S3. Comparison of plasma lipoprotein and triglyceride levels in 4mo old severe mdx mice fed either a standard HFD or CHOL diet.

Video S1. Supporting information

Conflict of interest

The authors have declared that no conflict of interest exists.

References

1. Burch PM, Pogoryelova O, Goldstein R, Bennett D, Guglieri M, Straub V, et al. Muscle-derived proteins as serum biomarkers for monitoring disease progression in three forms of muscular dystrophy. *J Neuromuscul Dis* 2015;**2**:241–255.
2. Kornegay JN, Childers MK, Bogan DJ, Bogan JR, Nghiem P, Wang J, et al. The paradox of muscle hypertrophy in muscular dystrophy. *Phys Med Rehabil Clin N Am* 2012;**23**: 149–172.
3. Birnkrant DJ, Bushby K, Bann CM, Alman BA, Apkon SD, Blackwell A, et al. Diagnosis and management of Duchenne muscular dystrophy, part 2: respiratory, cardiac, bone health, and orthopaedic management. *Lancet Neurol* 2018;**17**:347–361.
4. Birnkrant DJ, Bushby K, Bann CM, Apkon SD, Blackwell A, Colvin MK, et al. Diagnosis and management of Duchenne muscular dystrophy, part 3: primary care, emergency management, psychosocial care, and transitions of care across the lifespan. *Lancet Neurol* 2018;**17**:445–455.
5. Liu J, Aoki M, Illa I, Wu C, Fardeau M, Angelini C, et al. Dysferlin, a novel skeletal muscle gene, is mutated in Miyoshi myopathy and limb girdle muscular dystrophy. *Nat Genet* 1998;**20**:31–36.
6. Laval SH, Bushby KMD. Limb-girdle muscular dystrophies—from genetics to molecular pathology. *Neuropathol Appl Neurobiol* 2004;**30**:91–105.
7. Viollet L, Thrush PT, Flanigan KM, Mendell JR, Allen HD. Effects of angiotensin-converting enzyme inhibitors and/or beta blockers on the cardiomyopathy in Duchenne muscular dystrophy. *Am J Cardiol* 2012;**110**:98–102.
8. Bansal D, Miyake K, Vogel SS, Groh S, Chen CC, Williamson R, et al. Defective membrane repair in dysferlin-deficient muscular dystrophy. *Nature* 2003;**423**: 168–172.
9. Bansal D, Campbell KP. Dysferlin and the plasma membrane repair in muscular dystrophy. *Trends Cell Biol* 2004;**14**: 206–213.
10. van Putten M, Lloyd EM, de Greef JC, Raz V, Willmann R, Grounds MD. Mouse models for muscular dystrophies: an overview. *Dis Model Mech* 2020;**13**:dmm043562, https://doi.org/10.1242/dmm.043562
11. Milad N, White Z, Tehrani AY, Sellers S, Rossi FM, Bernatchez P. Increased plasma lipid levels exacerbate muscle pathology in the mdx mouse model of Duchenne muscular dystrophy. *Skelet Muscle* 2017; **7**:19.
12. Sellers SL, Milad N, White Z, Pascoe C, Chan R, Payne GW, et al. Increased nonHDL cholesterol levels cause muscle wasting and ambulatory dysfunction in the mouse model of LGMD2B. *J Lipid Res* 2018;**59**: 261–272.
13. Grainger DJ, Reckless J, McKilligin E. Apolipoprotein E modulates clearance of apoptotic bodies in vitro and in vivo, resulting in a systemic proinflammatory state in apolipoprotein E-deficient mice. *J Immunol* 2004;**173**:6366–6375.
14. White Z, Hakim CH, Theret M, Yang NN, Rossi F, Cox D, et al. High prevalence of plasma lipid abnormalities in human and canine Duchenne and Becker muscular dystrophies depicts a new type of primary genetic dyslipidemia. *J Clin Lipidol* 2020;**4**: 459–469 [published online ahead of print: May 2020].
15. Milad N, White Z, Tehrani AY, Sellers S, Rossi FM, Bernatchez P. Increased plasma lipid levels exacerbate muscle pathology in the mdx mouse model of Duchenne muscular dystrophy Skelet. *Muscle* 2017; **7**:19, https://doi.org/10.1186/s13395-017-0135-9
16. Altmann SW, Davis HR, Zhu LJ, Yao X, Hoos LM, Tetzloff G, et al. Niemann-Pick C1 Like 1 protein is critical for intestinal cholesterol absorption. *Science* 2004;**303**:1201–1204.
17. Grounds MD, Terrill JR, Radley-Crabb HG, Robertson T, Papadimitriou J, Spuler S, et al. Lipid accumulation in dysferlin-deficient muscles. *Am J Pathol* 2014;**184**:1668–1676.
18. Agarwal AK, Tunison K, Mitsche MA, McDonald JG, Garg A. Insights into lipid accumulation in skeletal muscle in dysferlin-deficient mice. *J Lipid Res* 2019; **60**:2057–2073.
19. Díaz J, Woudt L, Suazo L, Garrido C, Caviedes P, Cárdenas AM, et al. Broadening the imaging phenotype of dysferlinopathy at different disease stages. *Muscle Nerve* 2016;**54**:203–210.
20. Kobayashi K, Izawa T, Kuwamura M, Yamate J. The distribution and characterization of skeletal muscle lesions in dysferlin-deficient SJL and A/J mice. *Exp Toxicol Pathol* 2010;**62**:509–517.
21. Hammers DW, Hart CC, Matheny MK, Wright LA, Armellini M, Barton ER, et al. The D2.mdx mouse as a preclinical model of the skeletal muscle pathology associated with Duchenne muscular dystrophy. *Sci Rep* 2020;**10**:14070.
22. Chrzanowski SM, Baligand C, Willcocks RJ, Deol J, Schmalfuss I, Lott DJ, et al. Multi-slice MRI reveals heterogeneity in disease distribution along the length of muscle in Duchenne muscular dystrophy. *Acta Myol* 2017;**36**:151–162.
23. Wokke BH, Van Den Bergen JC, Versluis MJ, Niks EH, Milles J, Webb AG, et al. Quantitative MRI and strength measurements in the assessment of muscle quality in Duchenne muscular dystrophy. *Neuromuscul Disord* 2014;**24**:409–416.
24. Gaur L, Hanna A, Bandettini WP, Fischbeck KH, Arai AE, Mankodi A. Upper arm and cardiac magnetic resonance imaging in Duchenne muscular dystrophy. *Ann Clin Transl Neurol* 2016;**3**:948–955.
25. Mead AF, Petrov M, Malik AS, Mitchell MA, Childers MK, Bogan JR, et al. Diaphragm remodeling and compensatory respiratory mechanics in a canine model of Duchenne muscular dystrophy. *J Appl Physiol* 2014; **116**:807–815.
26. De Bruin PF, Ueki J, Bush A, Khan Y, Watson A, Pride NB. Diaphragm thickness and inspiratory strength in patients with Duchenne muscular dystrophy. *Thorax* 1997;**52**:472–475.
27. Desguerre I, Arnold L, Vignaud A, Cuvellier S, Yacoub-youssef H, Gherardi RK, et al. A new model of experimental fibrosis in hindlimb skeletal muscle of adult mdx mouse mimicking muscular dystrophy. *Muscle Nerve* 2012; **45**:803–814.
28. Soliman H, Paylor B, Scott RW, Lemos DR, Chang C, Arostegui M, et al. Pathogenic potential of Hic1-expressing cardiac stromal progenitors. *Cell Stem Cell* 2020;**26**: 205–220, e8.
29. Zhang Y, Parmigiani G, Johnson WE. ComBat-seq: batch effect adjustment for RNA-seq count data. *NAR Genom Bioinform* 2020;**2**:lqaa078.
30. Love MI, Huber W, Anders S. Moderated estimation of fold change and dispersion for RNA-seq data with DESeq2. *Genome Biol* 2014;**15**:550.
31. Yu G, Wang L-G, Han Y, He Q-Y. clusterProfiler: an R package for comparing biological themes among gene clusters. *OMICS* 2012;**16**:284–287.
32. Barrientos G, Sánchez-Aguilera P, Jaimovich E, Hidalgo C, Llanos P. Membrane cholesterol in skeletal muscle: a novel player in excitation-contraction coupling and insulin resistance. *J Diabetes Res* 2017;**2017**:3941898, 1, 8.
33. Yokoyama M, Seo T, Park T, Yagyu H, Hu Y, Son NH, et al. Effects of lipoprotein lipase and statins on cholesterol uptake into

heart and skeletal muscle. *J Lipid Res* 2007; **48**:646–655.
34. Spady DK, Dietschy JM. Sterol synthesis in vivo in 18 tissues of the squirrel monkey, guinea pig, rabbit, hamster, and rat. *J Lipid Res* 1983;**24**:303–315.
35. Osaki Y, Nakagawa Y, Miyahara S, Iwasaki H, Ishii A, Matsuzaka T, et al. Skeletal muscle-specific HMG-CoA reductase knockout mice exhibit rhabdomyolysis: a model for statin-induced myopathy. *Biochem Biophys Res Commun* 2015;**466**:536–540.
36. Wallace GQ, McNally EM. Mechanisms of muscle degeneration, regeneration, and repair in the muscular dystrophies. *Annu Rev Physiol* 2009;**71**:37–57.
37. Haynes VR, Keenan SN, Bayliss J, Lloyd EM, Meikle PJ, Grounds MD, et al. Dysferlin deficiency alters lipid metabolism and remodels the skeletal muscle lipidome in mice. *J Lipid Res* 2019;**60**:1350–1364.
38. Joe AWB, Yi L, Natarajan A, Le Grand F, So L, Wang J, et al. Muscle injury activates resident fibro/adipogenic progenitors that facilitate myogenesis. *Nat Cell Biol* 2010;**12**:153–163.
39. Etich J, Koch M, Wagener R, Zaucke F, Fabri M, Brachvogel B. Gene expression profiling of the extracellular matrix signature in macrophages of different activation status: relevance for skin wound healing. *Int J Mol Sci* 2019;**20**:5086, https://doi.org/10.3390/ijms20205086